THE ASTROPHYSICAL JOURNAL, 441:779–785, 1995 March 10

HARD X-RAY VARIABILITY OF X-RAY NOVA PERSEI 1992: *GRANAT*/SIGMA RESULTS

A. VIKHLININ, E. CHURAZOV, M. GILFANOV, R. SUNYAEV, A. FINOGUENOV, A. DYACHKOV, R. KREMNEV, AND K. SUKHANOV
Space Research Institute, Russian Academy of Sciences, Profsouznaya 84/32, 117810 Moscow, Russia
J. BALLET, A. GOLDWURM, B. CORDIER, AND A. CLARET
Service d'Astrophysique, Centre d'Etudes Nucleaires de Saclay, 91191 Gif-sur-Yvette Cedex, France
AND
M. DENIS, J. F. OLIVE, J. P. ROQUES, AND P. MANDROU
Centre d'Etude Spatiale des Rayonnements, 9, avenue du Colonel Roche, BP 4346, 31029 Toulouse Cedex, France
Received 1994 February 28; accepted 1994 September 20

ABSTRACT

Nova Persei 1992 (GRO J0422+32) was observed by *Granat*/ SIGMA in 1992 August–September, being at that time the brightest hard X-ray source detected by SIGMA. We have analyzed the source hard (40–150 keV) X-ray variability on timescales from days to seconds. From 1992 August 15 until September 25 the 40–150 keV decreased monotonically from 2.9 to 1.0 crab following an exponential decay law with an *e*-folding time of 43 days. On timescales of hours the source was remarkably stable: the rms variations with respect to the exponential fit are ≈3%. Power density spectra (PDSs) were obtained in the 10^{-4}–10 Hz frequency range. The power density is nearly constant below 0.03 Hz and decreases as a power law $f^{-\alpha}$ above this frequency, with an index $\alpha \simeq 0.9$. A significant decrease of power density below the frequency of about 3×10^{-3} Hz was seen during the first half of observations. A strong peak of quasi-periodic oscillations was detected at the frequency of 0.3 Hz, with associated rms variations of intensity ∼12%. The total fractional rms variations of the source flux in the 10^{-3}–10^{-1} Hz range were ∼15% during the first observations and increased to ∼25% as the source flux decreased. A shot noise model has been applied to describe the strong flickering of GRO J0422+32, and parameters of this model (shot amplitude, rate, and typical duration) have been determined from the analysis of the PDSs and the counts distribution.

Subject headings: novae, cataclysmic variables — stars: individual (Nova Persei 1992) — X-rays: stars

1. INTRODUCTION

A very bright X-ray transient (Nova Persei 1992, GRO J0422+32) was discovered by *CGRO*/BATSE on 1992 August 5 (Paciesas et al. 1992). The source intensity rose sharply and by August 8 reached the ≈3 crab level. *Granat*/SIGMA started observing GRO J0422+32 on August 15. The source was localized at R.A. = $4^h18^m27^s$, decl. = +32°48′0 (equinox 1950.0), with an error radius of about 2′ (Goldwurm et al. 1992), in agreement with the position obtained by *IUE* (Shrader et al. 1992). The hard source spectrum (Roques et al. 1994; Sunyaev et al. 1994) and the strong chaotic variability on short timescales resembled well the properties of two other bright X-ray novae (GS 2033+338: Sunyaev et al. 1991; Tanaka et al. 1989; Nova Muscae 1991 [GRS 1124−68]: Sunyaev et al. 1992; Goldwurm et al. 1992) and Cygnus X-1 (Sunyaev & Truemper 1979; Ling et al. 1987; Nolan et al. 1981). Since Cygnus X-1 GS 2033+338, and Nova Muscae 1991 are considered to be "reliable" black hole candidates, several authors (i.e., Sunyaev et al. 1993; Roques et al. 1994) suggested that Nova Persei was the fourth black hole candidate among bright X-ray novae (previously mass functions in excess of $\sim 3\ M_\odot$ have been reported for A06020−00 (McClintock & Remillard 1986), GS 2023+338 (Casares, Charles, & Naylor 1992) and GRS 1124−68 (Remillard, McClintock & Bailyn 1992).

In this paper we report the results of a timing analysis of GRO J0422+32. Observations were carried out with *Granat*/ SIGMA from 1992 August 15 until September 25.

2. INSTRUMENT AND OBSERVATIONS

The SIGMA hard X-ray/soft γ-ray telescope is one of two main imaging instruments on board the *Granat* orbital observatory. It is designed to obtain sky images in the 35–1300 keV energy band as well as perform timing analysis of hard X-ray emission. The FWHM of the telescope field of view is an 11°.5 by 10°.6 rectangle of which a 4°.7 by 4°.3 area corresponds to the fully coded field of view with constant sensitivity. The geometrical area of the NaI(Tl) position sensitive detector is 794 cm^2. A detailed description of the telescope is given by Paul et al. (1991).

In total, 15 observations of GRO J0422+32 were carried out with the SIGMA telescope (Table 1), and two operational modes were used: the Standard Spectroscopy/imaging mode and the timing mode. In the Spectroscopy/imaging mode three types of scientific information are recorded into the on-board memory: (1) the "fine images" (FIs), images of the detector in four broad spectral bands with 1′.6 pixel size and exposure from 1 to 4 hr.; (2) the "spectral images" (SIs), images of the detector in 95 adjacent spectral channels with 3′.2 pixel size and exposure time twice that for the FIs; and (3) the "4 s count rates," the number of counts detected by the entire detector (without spatial information) in four spectral bands (the same as for FI) with a time resolution of 4 s, uninterrupted over the whole session. The typical duration of an observational session in the Spectroscopy/Imaging mode is ∼20 hr. For the timing analysis reported below, the 4 s count rates have been used.

One of the observations (498, 1992 Aug 22) was performed in

TABLE 1

LIST OF OBSERVATIONS OF GRO J0422+32 WITH *GRANAT*/SIGMA

Observation Number	Date (UT)		Duration (hr)
493.....	1992 Aug	15.77–16.58	19.
494.....	1992 Aug	16.71–17.44	18.
495.....	1992 Aug	17.58–18.81	30.
496.....	1992 Aug	20.48–21.38	22.
498[a].....	1992 Aug	22.39–22.51	3.1
499.....	1992 Aug	24.49–25.44	23.
500.....	1992 Aug	25.55–26.30	18.
501.....	1992 Aug	26.43–27.03	14.
503.....	1992 Aug	29.56–30.28	17.
504.....	1992 Sep	1.45–2.42	23.
505.....	1992 Sep	2.55–3.29	18.
506.....	1992 Sep	3.41–4.22	19.
507.....	1992 Sep	5.47–6.68	43.
508.....	1992 Sep	13.48–14.38	22.
517.....	1992 Sep	25.81–26.46	16.

[a] In "Timing" mode.

the Timing mode. In this mode the count rate of the whole detector is recorded with 1/1024 s time resolution. Energies of each photon are determined, but no imaging information is available. The duration of observations carried out in the Timing mode is equal approximately to 3 hr, restricted by the capacity of the on-board memory.

3. LIGHT CURVE

The light curve of Nova Persei in the 40–150 keV energy band extracted from the FI exposures with ~3 hr time resolution is shown in Figure 1*a*. The hard X-ray intensity of GRO J0422+32 decreased very smoothly during the course of the SIGMA observations from 2.9 to 1.0 crab (which corresponds to a decrease of the luminosity from 4.5 to 1.7 × 10^{36} ergs s^{-1} in the 40–150 keV band, assuming the distance to the source is 1 kpc). The data shown in Figure 1 can be modeled by an exponential law ($e^{-t/\tau}$) with an *e*-folding time of about 40–45 days (Table 2). It can be seen from Table 2 that the flux in the 70–150 keV band decreased somewhat slower than that in the 40–70 keV band. This spectral evolution is clearly demonstrated by the time history of the hardness ratio (40–70 keV/70–150 keV flux; see below).

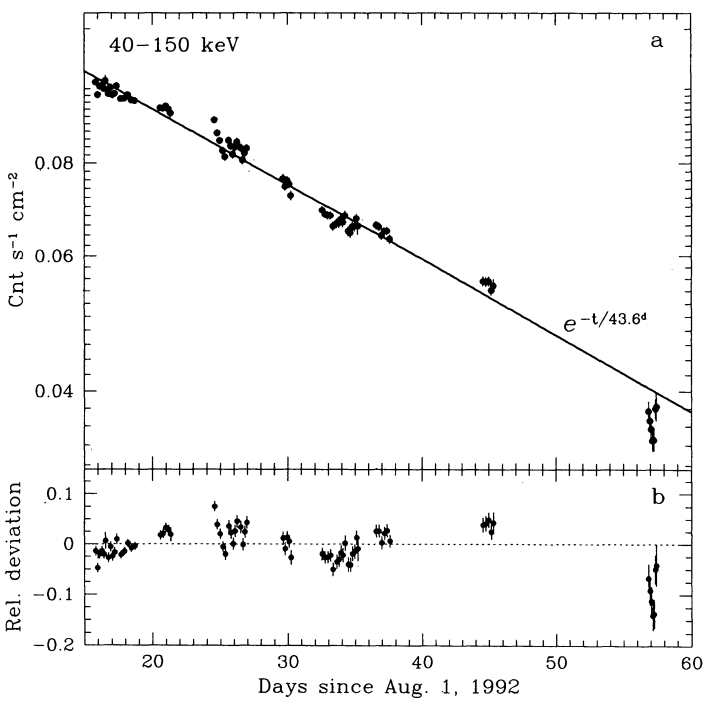

FIG. 1.—(*a*) 40–150 keV count rate determined from individual FI exposures. The solid line represents the best exponential fit. (*b*) Relative deviations of the data points from the exponential fit.

TABLE 2

e-FOLDING TIME FOR EXPONENTIAL FITS OF THE LIGHT CURVE

Energy Band	*e*-folding time (days)
40–150 keV.....	43.6 ± 0.7
40–70 keV.....	41.2 ± 0.9
70–150 keV.....	46.2 ± 0.9

The stability of the 40–150 keV flux on timescales of hours is remarkable. Over more than 1 month of observations rms variations of intensity around the exponential fit are equal to 3.6%, with maximum deviations of +7.5% and −14%. The residuals for the individual data points with respect to the exponential fit are shown in Figure 1*b*. This variability does not look like chaotic exposure-to-exposure variations of intensity, but rather an observation-to-observation (i.e., day-to-day) trend. The variations of intrinsic detector parameters (such as energy gain) from session to session could be on the level of percents, giving a nonnegligible contribution to the observed intensity variations. So to be conservative, one should treat the value of 3.6% as an upper limit to the intrinsic variations of the source flux on timescales of hours. This is completely different from the behavior of the other bright X-ray nova GRS 1125−68 (Sunyaev et al. 1992; Goldwurm et al. 1992), which was variable by a factor of ~2 on timescales of hours.

4. POWER DENSITY SPECTRA

4.1. *Data Reduction*

In order to study the variability of the hard X-ray flux of Nova Persei on timescales from 10^3 to 0.1 s, power density spectra (PDSs) have been calculated via standard Fourier techniques (van der Klis 1989). For each SI observation the 4 s count rates have been divided into samples of 1024 bins (4 s long). The data obtained in the Timing mode (session 498) were grouped into samples of 4096 bins, 80 ms duration each. The PDSs obtained for individual samples were averaged over each observational session. After standard normalization (Leahy et al. 1983), the Poisson noise contribution has been subtracted. The PDSs derived from the data of the Spectroscopy/Imaging observations were also corrected for the "diffraction" effect (drop of efficiency near the Nyquist frequency). Using the source intensity in the same energy band, obtained from imaging data of the same session, the PDSs were renormalized to units of squared fractional rms variations density (Hz^{-1}). To obtain the intensity of GRO J0422+32 during session 498 ("Timing" mode) we interpolated the count rate records of the two neighboring observations. The interpolated intensity seems to be valid, as the power spectra derived from the data of the Timing and the Spectroscopy/Imaging observations are in good agreement in the overlapping frequency range (Fig. 2).

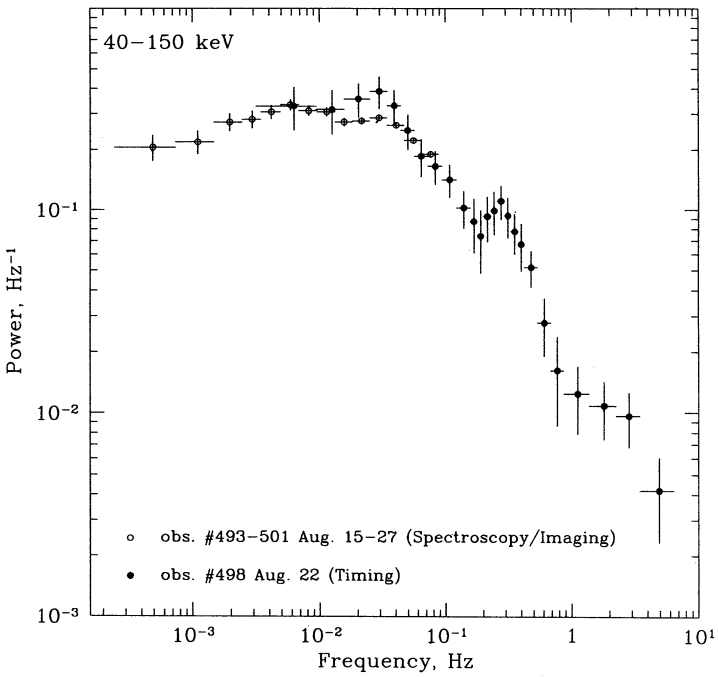

FIG. 2.—PDS of GRO J0442+32 40–150 keV flux. Solid circles correspond to the data of the Timing observation (498), and open circles to the first seven (493–501) sessions in the Spectroscopy/Imaging mode.

There are two effects which contribute to the uncertainty of PDSs: (1) Poisson fluctuations of the number of detected photons and (2) the random variability of a source itself (van der Klis 1989). For a weak source, the first effect dominates, while for a bright, highly variable source neglecting the second effect leads to the underestimation of error bars and unacceptably high values of χ^2 for power spectra fits. Accounting for both effects, the standard deviation of $\langle P_i \rangle$ is $\sigma_i = (2 + \langle P_i \rangle)/(n)^{1/2}$, where $\langle P_i \rangle$ is the mean value of the power density at the given frequency after normalization according to Leahy et al. (1983), and n is the number of averaged spectra. When the number of averaged spectra is large enough ($n^{1/2} \gg 1$) the estimation of σ_i can be based on the *measured* value of $\langle P_i \rangle$; the corresponding error bars are shown in Figures 2–3 (note that this method fails in the case of moderate n because of poor accuracy and correlation of values of σ_i and $\langle P_i \rangle$).

In order to estimate the total power of the variable component over a given frequency range, the total fractional rms variations have been calculated as the sum of power densities at all frequencies in this range:

$$\mathrm{rms}^2 = (\sum P_i \Delta f_i) C/S^2 ,$$

where C and S are the total and source count rates, respectively.

4.2. 0.3 Hz *Quasi-Periodic Oscillations*

The PDS in a wide frequency range (3.6×10^{-4}–12.5 Hz) obtained from the data of the first eight observations (one of which was performed in the Timing mode) is shown in Figure 2. Above 0.03 Hz the PDS decreases as a power law with a superposed strong peak of quasi-periodic oscillations (QPOs) centered at about 0.3 Hz *CGRO*/BATSE detected the QPO at nearly the same frequency (Kouveliotou, Finger, & Fishman 1992b).

A simple model of power law + Lorentzian line has been applied to the data in the 0.03–5 Hz and 40–150 keV range (only the data obtained in session 498 were used). The fitting procedure was based on a maximum likelihood technique. The likelihood function is $L = \Pi 1/(2\pi\sigma_i^2)^{1/2} \exp [-(P_i - P_i^{(\mathrm{fit})})^2/2\sigma_i^2]$, with $\sigma_i = [2 + P_i^{(\mathrm{fit})}]/(n)^{1/2}$, which takes into account intrinsic source variability (see § 4.1). The significance of the QPO detection has been estimated from the ratio of likelihoods for best-fit models with and without the QPO peak; there is only a 9.5×10^{-5} probability of a "by chance" appearance of the QPO peak ($2\Delta \log L = 21.2$). Application of a maximum likelihood technique to power spectra fits is motivated by the contribution of a source variability to the values of statistical errors in power spectra. Traditional χ^2 minimization yields a biased estimation of fit parameters, when errors σ_i depend on fit values. The application of a maximum likelihood method to power spectra fits is discussed in more detail in Vikhlinin et al. (1994).

Best-fit parameters of the model are given in Table 3. The error bars on the parameters (the 68% single-parameter confidence intervals) have been determined from Monte Carlo simulations: for the best-fit model power spectrum we simulated 100 sets of "data points" [distributed according to the Gaussian distribution with $\sigma_i = (2 + P_i^{(\mathrm{fit})})/(n)^{1/2}$; see § 4.1], fitted each of the simulated power spectra, and then determined the 68% confidence regions for the model parameters.

QPOs in GRO J0422+32 is the fifth example of QPOs in black hole candidates (previously, QPOs in LMC X-1; [Ebisawa, Mitsuda, & Inoue 1989], GX 339−4 [Grebenev et al. 1991b; Dotani 1992], Nova Muscae [Grebenev et al. 1991a; Tanaka et al. 1991], and Cygnus X-1 [Vikhlinin et al. 1994; Kouveliotou, Finger, & Fishman 1992a; Angellini, White, & Stella 1992] have been reported). The observed QPO frequencies of black hole candidates (typically $\lesssim$ few 10^{-1} Hz, with the exception of Nova Muscae 1991) tend to be lower than those of low-mass X-ray binaries (LMXBs) ($\gtrsim$ few Hz). A comparison between variability properties of neutron stars and black hole candidates is given in a review by van der Klis (1994).

4.3. *Very Low Frequency Decline*

The shape of the 40–150 keV PDS at low frequencies exhibited some evolution during the whole set of SIGMA observations. The PDS in the 3×10^{-4}–0.1 Hz range averaged over observations from 1992 August 29 to September 26 can be well approximated by a constant below $\sim$0.03 Hz (Figure 3). In addition to a significantly lower level of power density, the PDS averaged over previous observations from August 15 to August 27 (shown in Fig. 3 by solid circles) exhibits significant turnover at low frequencies (less than $\sim 3 \times 10^{-3}$ Hz). To describe that in more detail, and estimate the significance of the very low frequency decline, we modeled the PDS in the 10^{-4}–3×10^{-2} frequency range. The model consisted of a power law

TABLE 3

BEST-FIT PARAMETERS OF THE QUASI-PERIODIC OSCILLATION PEAK

Parameter	Value
QPO frequency f_c (Hz)	0.31 ± 0.02
FWHM (Hz)	$0.16^{+0.09}_{-0.04}$
Fractional rms variations in QPO	$12.3^{+7.0}_{-3.5}$%
Power-law slope α	0.89 ± 0.05

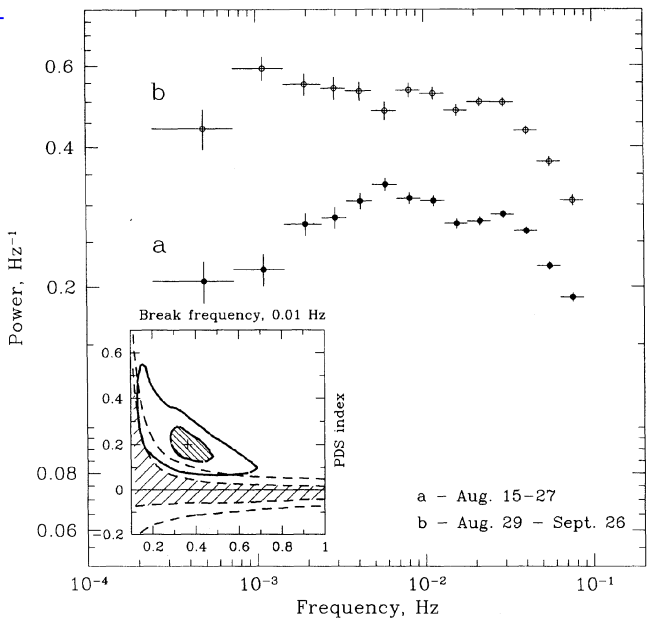

FIG. 3.—PDS averaged over the first (493–501) and the second (503–517) halves of the observations (curves a and b, respectively). Shown in the inset graph are zones of 68% and 95% confidence level for the low-frequency break frequency and the power-law index (*solid lines* correspond to the data of sessions 493–501 and *dashed lines* to sessions 503–517).

below the break frequency f_{br} and constant above this frequency. The break frequency, power density at this frequency, and the low frequency power-law index are free model parameters. The inset graph in Figure 3 shows two-dimensional zones corresponding to the confidence levels of 68% and 95% for values of the break frequency and the power-law index determined from the analysis of the likelihood function. While the PDS averaged over August 29 to September 26 observations is fully compatible with a constant level in the 10^{-3}–3×10^{-2} Hz frequency range (*dashed lines* in the inset graph), the presence of a decline of power density below 3.5×10^{-3} Hz in the data of the first seven observations (*solid lines* in the same figure) can be stated with the confidence of $\approx 99.8\%$. At lower frequencies (5×10^{-5}–2×10^{-4} Hz) the power spectrum is dominated by variations of the detector background; a 1 σ upper limit for the power density of GRO J0422+32 is 0.2 Hz^{-1}.

Such a decrease toward low frequencies seems to be rather unusual: typically PDSs exhibit strong very low frequency noise or at least remain at a constant level (a number of PDSs of Galactic X-ray sources can be found, for example, in Belloni & Hassinger 1990). The turnover of the PDS below 3.5×10^{-3} Hz suggests that the source intensity becomes more or less regular on timescales longer than 300 s. An example of such a behavior can be found in Angelini (1989), where a decrease of the PDS of the X-ray pulsar SMC X-1 toward low frequencies was accounted for through flaring activity of the source with a characteristic repetition time of ~ 100 s.

4.4. *Source Variability Versus Energy and Intensity*

It is usually considered that the variability in the light curves of black hole candidates consist of numerous overlapping flares (shots). It is possible to use power spectra derived in different energy bands to characterize the energy spectrum of flares. This technique does not require well time-resolved spectral observations of single flares, which usually fail because of Poisson fluctuations and overlapping of shots. Unfortunately, the power spectra cannot be used for determinations of energy spectra of a variable component, if variability waveforms in different energy bands are not the same. Suppose, for example, that the shots have exponential form, and that their amplitude and the e-folding time change with energy, i.e., an individual flare observed at different energies, can be described as $h(t) = A(E) \exp [-t/\tau(E)]$. In this case, the energy spectrum of the variable component would be proportional to $A(E)\tau(E)$, while the power spectrum normalization changes with energy as $A^2(E)\tau(E)$. If $\tau(E) \neq$ const, the power spectrum normalization cannot be used as a measure of energy spectrum of shots. The other possible model for the difference of variability waveforms in different energy bands is as follows. Suppose that the exponential shots have the same τ at each energy, but there is a number of hard flares, which are not observed at soft energies. In this case, the energy spectrum of the variable component would be proportional to $A(E)\nu(E)$, where $\nu(E)$ is the number of shots per unit time as a function of energy. Contrary to the energy spectrum, the power spectrum normalization is proportional to $A^2(E)\nu(E)$, and it is clear that if $\nu(E) \neq$ const, the power spectrum technique fails. Therefore, one should make sure that the variability waveforms at different energies are the same before using power spectra for the determination of the energy spectrum of variability components. If the first of the possibilities considered above is the case, the power spectra shape would be different at different energies. A good check for the second possibility is to determine the correlation coefficient between the light curves measured in the soft and the hard energy bands. If $\nu(E) \neq$ const, the correlation coefficient would be significantly less than unity.

To investigate the dependence of the PDS shape on the energy, we derived PDSs of the source intensity in two broad bands: 40–70 and 70–150 keV, using the data of observations 498 (Timing) and 496 and 499 (Spectroscopy/Imaging). The power spectra were modeled with a function consisting of a constant below a "break" frequency f_{br}, a power law $f^{-\alpha}$ above this frequency, and a Lorentzian function to describe a QPO peak. The best-fit values of the break frequency and the power-law index in the softer band ($f_{br} = 0.038 \pm 0.007$ Hz, $\alpha = 0.9 \pm 0.2$) and in the harder band ($f_{br} = 0.043 \pm 0.009$ Hz, $\alpha = 0.9 \pm 0.3$) are fully consistent. Determination of the correlation coefficient for intensity variations in these two bands gives the value of 0.98 ± 0.03, the 2 σ lower limit of 0.93. From such an analysis we conclude that the variability waveforms in the hard and soft energy bands are consistent within the statistics, and therefore, the power spectra can be used to determine the energy spectrum of short-term variations.

Using the Timing data we computed fractional rms variations as a function of energy (Fig. 4). No significant differences were found in the energy spectra of the QPOs (0.125–0.5 Hz) and the low-frequency noise (LFN) (below 0.125 Hz). The spectra are similar to each other and are clearly distinguished from the spectrum of total flux, suggesting both phenomena (QPO and LFN) to be of common origin.

The evolution of the "noise" spectrum time has been studied using the data from the Spectroscopy/Imaging observations by computing the hardness ratio of the variable component (i.e., the ratio of the 2.4×10^{-4}–0.08 Hz fractional rms variations of the 70–150 to the 40–70 keV flux). The variable

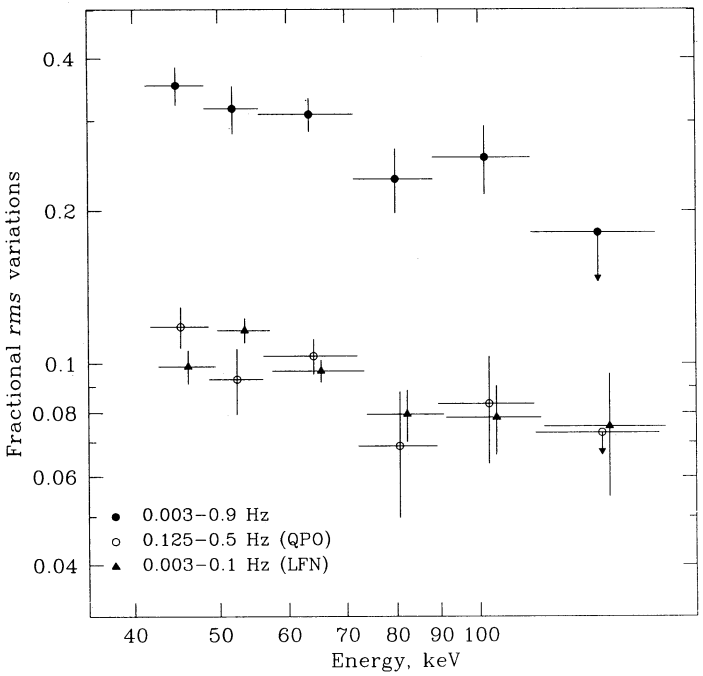

FIG. 4.—Fractional rms variations vs. energy dependence obtained from the Timing data (498). Open circles and triangles represent the spectra of the low-frequency noise (LFN) and the QPO, respectively.

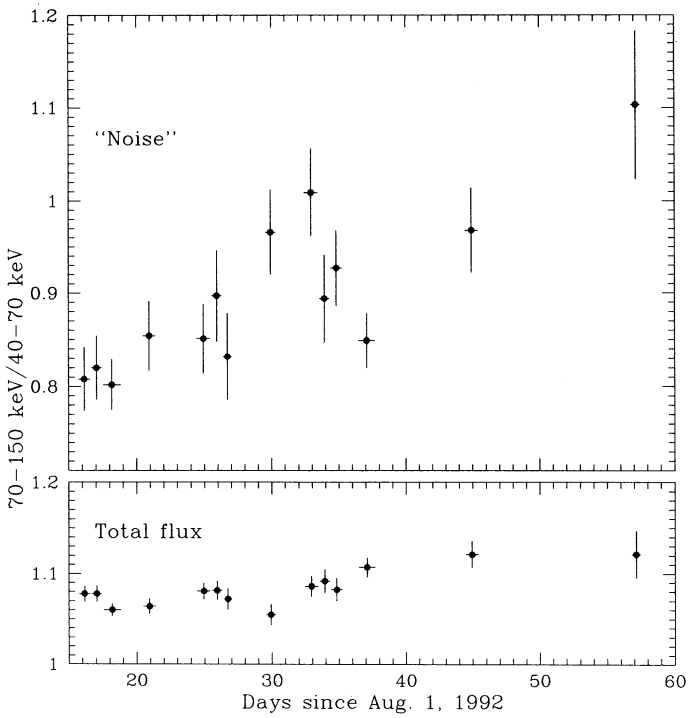

FIG. 5.—Hardness ratio (70–150 keV/40–70 keV) of (*a*) 3.6×10^{-4}–8×10^{-2} fractional rms variations, and (*b*) total flux.

component is significantly softer than the total flux during the first sessions (including 498); however, it became at least as hard as the overall source emission by the end of September (Fig. 5*a*). The values of the "noise" hardness ratio averaged over the first and second halves of the observations are equal to 0.82 ± 0.02 and 0.94 ± 0.03, respectively. The hardness ratio of the total flux also increased with time (Fig. 5*b*), as can be expected from comparison of the characteristic decay times of the source flux in the two energy bands (§ 3, Table 2). The high value of the fraction of variable component ($\geq 25\%$, § 5) suggests that the increase in the hardness ratio was caused by the hardening of the spectrum of the variable component.

The values of the fractional rms variations of the 40–150 keV flux of Nova Persei in the 10^{-3}–0.1 Hz frequency range obtained in individual sessions are shown in Figure 6. The decrease of the source flux in this energy band by a factor of 3 from August 15 until September 25 was accompanied by a ≈ 1.7 times increase of the total fractional rms variations. The time evolution of the fractional rms value roughly follows $C_0^{-0.67}$ (shown in Fig. 6 by *open circles*). Some implications of the correlation between the source variability and intensity are discussed in the end of the next section.

5. SHOT NOISE PARAMETERS

Flickering in the X-ray count rate record of various sources, which is similar to that observed from Cygnus X-1, is commonly interpreted to be due to a shot noise (SN) process. A rather good agreement of the SN model with the observed data can be achieved after introducing a distribution of shot duration and amplitude (Belloni & Hasinger 1990; Lochner, Swank, & Szymkowiak 1991). A power spectrum analysis fails in determining characteristics of the SN process such as shot rate and mean amplitude because the same shape of PDS (and the same value of fractional rms) can be reproduced for a variety of these parameters. Because of the possibility of strong overlap, direct observations of individual shots from high–time resolution data may also provide invalid results.

We tried to determine the region in the shot rate (λ)–shot amplitude (A) diagram, where the values of the parameters are

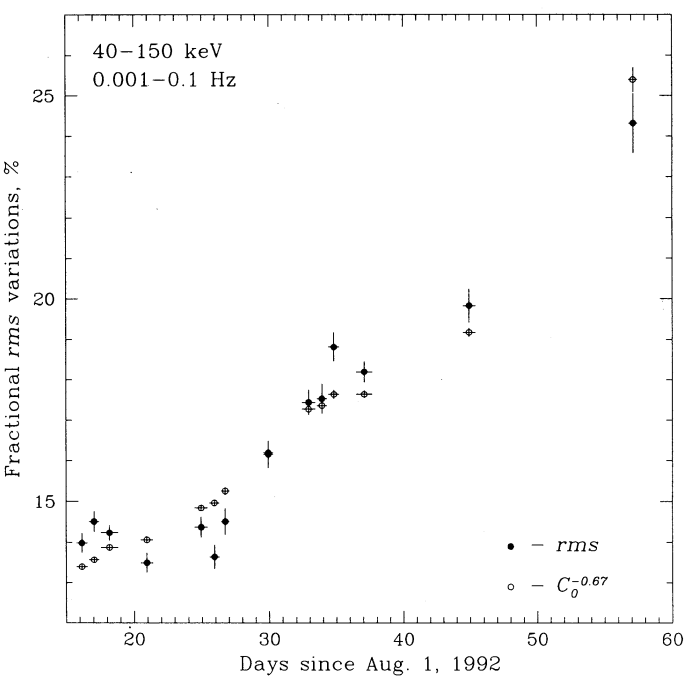

FIG. 6.—3.6×10^{-4}–8×10^{-2} fractional rms variations of the 40–150 keV flux evolution vs. source luminosity (*open circles* correspond to the values of $CL^{-0.67}$).

consistent with the SIGMA data. To make the calculations independent of a particular shot shape, $h(t)$, some integral characteristics of shots were used; total power ϵ, amplitude A, and duration τ, which are defined as follows:

$$\epsilon = \int_{-\infty}^{\infty} h(t)dt\,, \tag{1}$$

$$A = \max_t h(t)\,, \tag{2}$$

$$\tau = \epsilon/A\,. \tag{3}$$

Such a definition of a timescale, τ, of course, requires that no substructure be present in the shot shape [i.e., $h(t + \Delta t) - h(t) \ll h(t)$ for $\Delta t \ll \tau$].

The next two equations (4) and (6), obtained under the assumption that all shots have the same shape and duration, set some restrictions on the parameters of the SN process based on the directly measured quantities: the source flux and its rms variations. First, the count rate due to shots, $C_{sh} = \epsilon\lambda$, cannot exceed total source flux C_0, i.e.,

$$A \le C_0/(\lambda\tau)\,. \tag{4}$$

Using the expression for the fractional rms variations, we set another restriction on the amplitude. If $v(t)$ is the variable component of intensity, $v(t) = \Sigma h(t - t_k)$, then by definition,

$$\mathrm{rms}^2 = \lim_{T\to\infty} \frac{\int_0^T [v(t) - C_{sh}]^2\,dt}{\int_0^T C_0^2\,dt} = \left(\frac{\lambda}{C_0^2}\right)\int_{-\infty}^{\infty} h^2(t)dt\,. \tag{5}$$

Obviously, $\int_{-\infty}^{\infty} h^2(t)dt \le A\int_{-\infty}^{\infty} h(t)dt$, and finally,

$$A^2 \ge \frac{C_0^2\,\mathrm{rms}^2}{\lambda\tau}\,. \tag{6}$$

Thus, regardless of the particular shape of the shots, the parameters of the SN process (relative shot amplitude A/C_0 and overlap parameter $\lambda\tau$) lie inside a "beak" restricted by the two curves: $A/C_0 = 1/(\lambda\tau)$ (eq. [4]) and $(A/C_0)^2 = \mathrm{rms}^2/(\lambda\tau)$ (eq. [6]). For a given value of the rms, the minimal relative shot amplitude is $A/C_0 = \mathrm{rms}^2$, and the maximal shot overlap parameter is $\lambda\tau = 1/\mathrm{rms}^2$. Figure 7 shows the "beak," which corresponds to the value of the rms flux variations actually measured for GRO J0422+32 at the date of the Timing observation (30% in 0.001–5 Hz frequency range) shown in Figure 7.

Next, we considered the distribution of the number of counts per time bin. This distribution is determined by (1) Poisson scattering of counts around the mean value and (2) intrinsic intensity variations. If shots are strongly overlapping ($\lambda\tau \gg 1$), the intensity variations will follow a Gaussian distribution (central limit theorem). On the contrary, rare shots should be of large amplitude (eq. [7]) making the intensity distribution non-Gaussian. Thus, the analysis of the counts distribution gives information about shot rate and amplitude. We have simulated the counts distribution for rectangular and exponential shots and compared it to that actually measured during the "Timing" observation. The typical shot duration was fixed at 1 s, slightly longer than that given by the FWHM of our power spectrum (~2 s) to take into account the existence of more rapid fluctuations. The time bin was set at 1 s (values close to 1 s were found in numerous runs to be the most effective for the analysis of shots with duration of the order of 1 s). For a

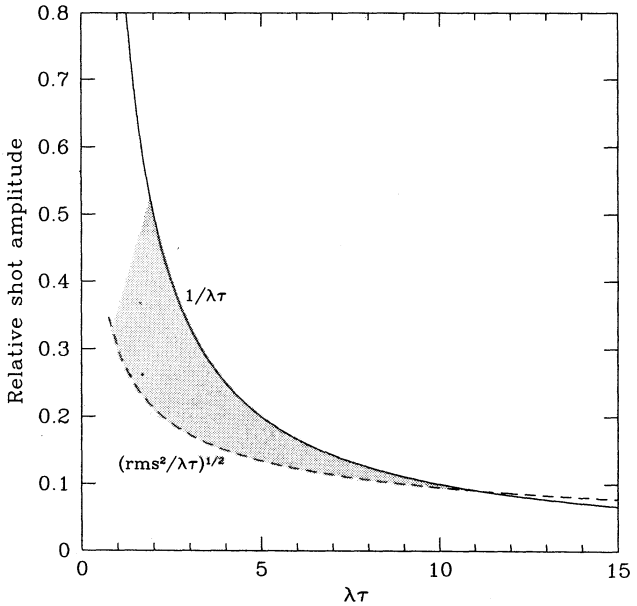

FIG. 7.—Relative amplitude (A/C_0)–shots overlap parameter ($\lambda\tau$) diagram. Region of possible SN parameters is shaded.

number of values of the shot rate, λ, the shot amplitude was calculated as $A = [\mathrm{rms}^2 C_0^2/(\lambda\tau)]^{1/2}$ for a rectangular shape, and $A = [2\ \mathrm{rms}^2 C_0^2/(\lambda\tau)]^{1/2}$ for an exponential shape; in each case, counts distribution has been simulated. The simulated and measured distributions have been compared using Pearson's χ^2 value (in five rather broad intensity bins). Shown in Figure 8 are values of χ^2 versus $\lambda\tau$ values for rectangular and exponential shots. The 90% lower limit of $\lambda\tau$ (*dashed line* in Fig. 8) is equal to 0.85 for rectangular and 1.2 for exponential

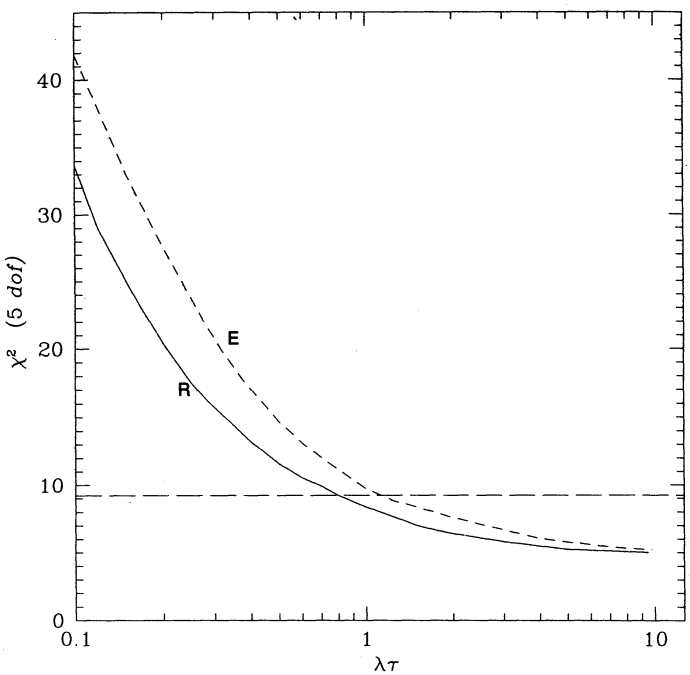

FIG. 8.—Values of Pearson's χ^2 (5 d.o.f.) for the measured distribution of photons per time bin for the exponential (E) and rectangular (R) shots. The horizontal line shows the 90% upper limit of the values of χ^2_5 distribution.

shots. Finally, the zone of possible SN parameters is shaded in Figure 7; the left boundary is a straight line drawn by joining the two points obtained in Figure 8.

Some conclusions about SN properties can be drawn from this analysis. First, shots contribute significantly to the total luminosity of the source: their fraction is at least 28%, and their amplitude exceeds at any rate 9% of the mean source intensity. Shots are overlapping (the value of $\lambda\tau$ is probably larger than 1, see Fig. 7), indicating that the instability responsible for the flickering activity should be local. The phase portrait analysis of the *HEAO 1* A-2, and *EXOSAT* ME data by Lochner et al. (1991) revealed that the phase portrait of the Cyg X-1 light curve requires that shots should contribute $\sim 50\%$ of the flux, and the overlap parameter is of the order or greater than unity.

Finally, we present some considerations of the evolution of SN parameters, based on the data presented in the previous section. Since the global shape of the PDS was more or less stable over all the SIGMA observations (Denis et al. 1994), we can assume that the shape and duration of the shots is independent of the source luminosity. Then the total fractional rms variations will be proportional to $A^{1/2}\varphi^{1/2}/C_0^{1/2}$, where A is the shot amplitude and φ is the fraction of the variable component in the total source flux C_0. The time evolution of the fractional rms value roughly follows $C_0^{-0.67}$ (Fig. 6), indicating that $A^{1/2}\varphi^{1/2} \approx C_0^{-0.17}$ slowly changes with the decrease of the source intensity. This means, for example, that if the shot fraction is kept the same, then the shot rate (rather than the amplitude) decreases with the total flux. If, on the contrary, the amplitude A changes strongly with the decrease of luminosity, then the fraction of the variable component should vary as $\varphi \sim 1/A$.

6. CONCLUSIONS

In this paper we report the analysis of time variability properties of the hard X-ray emission from Nova Persei 1992 (GRO J0422+32). Our main results can be summarized as follows.

During 1 month of observations, the changes of the source intensity can be well described by an exponential decay model with an e-folding time of 43 days (the relative rms variations around the fit are less than 3.6%). Unlike several other hard X-ray sources (e.g., Cyg X-1 and Nova Muscae 1991) GRO J0422+32 was remarkably stable on a timescale of hours.

PDSs of the 40–150 keV flux, measured in the 3.4×10^{-4}–10 Hz frequency range, revealed the presence of a strong peak of QPOs near 0.3 Hz. The value of fractional rms variations indicates that the QPO contributes $\sim 10\%$ of the source intensity. This is the fifth example of QPO detection from black hole candidates.

A significant lack of power was observed at the very low frequencies (below 3×10^{-3} Hz) during the first eight observations of GRO J0422+32. Thus, there should be a characteristic time of 300 s in the source intensity variations.

Sufficient energy resolution of the Timing data enabled us to build a "noise" energy spectrum which turned out to be significantly softer than that of the total flux on the date of the Timing observation (1992 August 22). LFN and QPO energy spectra are fully compatible, and the fact that they are clearly distinguished from the spectrum of the total flux suggests a common origin for both phenomena.

Both the "noise" spectrum and the value of the fractional rms variations evolved significantly during 1 month of SIGMA observations. The fractional rms dependence on the source flux roughly followed $L^{-1/2}$. This result can be easily interpreted in the framework of a SN model, implying that the shot rate (rather than amplitude) follows the changes of the luminosity. The energy spectra of the "noise" and the total flux simultaneously hardened during the course of the SIGMA observations.

If the short-term variability is interpreted as SN, significant restrictions can be set on the possible values of shot rate and amplitude from the analysis of the PDS and the distribution of counts. This analysis shows that shots should contribute significantly to the total source flux: their fraction exceeds at any rate 25% of the hard X-ray luminosity. The fact that shots do overlap indicates that the instability in the accretion disk responsible for the flickering is local.

We would like to thank an anonymous referee who suggested numerous improvements to the original text. This work was partially supported by a grant from the Russian Fundamental Research Foundation (93-02-17166), and by grant M7M000 from the International Science Foundation.

REFERENCES

Angelini, L. 1989, in Proc. 23d ESLAB Symp. ed. J. Hunt & B. Battrick (ESA SP-296, 1, 81)
Angelini, L., White, N. E., & Stellar, L. 1992, IAU Circ., No. 5580
Belloni, T., & Hasinger, G. 1990, A&A, 227, L33
Casares, J., Charles, P. A., & Naylor, T. 1992, Nature, 355, 614
Denis, M., et al. 1994, ApJS, 92, 459
Dotani, T. 1992, in Frontiers of X-ray Astronomy, ed. Y. Tanaka & K. Koyama (Tokyo: Universal Academy), 151
Ebisawa, K., Mitsuda, K., & Inoue, H. 1989, PASJ, 41, 159
Goldwurm, A., et al. 1992, ApJ, 389, L79
Grebenev, S., Sunyaev, R., & Pavlinsky, M. 1991a, GRI preprint 2–91, 125
Grebenev, S., Sunyaev, R., Pavlinsky, M., & Dekhanov, I. 1991b, Soviet Astron. Lett., 17, 985
Harmon, B. A., et al. 1993, IAU Circ., No. 5685
Kouveliotou, C., Finger, M. H., & Fishman, G. J. 1992a, IAU Cir., No. 5576
———. 1992b, IAU Circ., No. 5592
Leahy, D. A., Darbro, W., Elsner, R. F., Weisskopf, M. C., Sutherland, P. G., Kahn, C., & Grindlay, J. E. 1983, ApJ, 266, 160
Ling, J., et al. 1987, ApJ, 321, L117
Lochner, J. C., Swank, J. H., & Szymkowiak, A. E. 1991, ApJ, 376, 295
McClintock, J. E., & Remillard, R. A. 1986, ApJ, 308, 110
Nolan, P. L., et al. 1981, ApJ, 246, 494
Paciesas, W. S., et al. 1992, IAU Circ., No. 5580
Paul, J., et al. 1991, Adv. Space Res., 11, 289
Remillard, R., McClintock, J., & Bailyn, C. 1992, ApJ, 399, L145
Roques, J.-P., et al. 1994, ApJS, 92, 451
Shrader, C. R., et al. 1992, IAU Circ., No. 5591
Sunyaev, R. A., & Truemper, J. 1979, Nature, 279, 506
Sunyaev, R. A., et al. 1991, Sov. Astron. Lett., 17, 29
———. 1992, ApJ, 389, L95
———. 1993, A&A, 280, L1
Tanaka, Y. 1989, in Proc. 23d ESLAB Symp., ed. J. Hunt & B. Battrick (ESA SP-296, 1, 3)
Tanaka, Y., et al. 1991, in Proc. of Workshop on Nova Muscae, ed. S. Brandt (NATO ASI Ser., C262, p. 19)
van der Klis, M. 1989, in Timing Neutron Stars, ed. H. Ögelman & E. P. J. van den Heuvel (NATO ASI Ser., C262, p. 27)
———. 1994, ApJS, 92, 511
Vikhlinin, A., et al. 1994, ApJ, 424, 395